The Catalytic and Conformational Cycle of *Aquifex aeolicus* KDO8P Synthase: Role of the L7 Loop[†,‡]

Xingjue Xu,[§] Fathima Kona,[§] Jian Wang, Jinshuang Lu, Timothy Stemmler, and Domenico L. Gatti*

Department of Biochemistry and Molecular Biology, Wayne State University School of Medicine, Detroit, Michigan 48201

Received June 8, 2005

ABSTRACT: KDO8P synthase catalyzes the condensation of arabinose 5-phosphate (A5P) and phosphoenolpyruvate (PEP) to form the 8-carbon sugar KDO8P and inorganic phosphate (P_i). The X-ray structure of the wild-type enzyme shows that when both PEP and A5P bind, the active site becomes isolated from the environment due to a conformational change of the L7 loop. The structures of the R106G mutant, without substrates, and with PEP and PEP *plus* A5P bound, were determined and reveal that in R106G closure of the L7 loop is impaired. The structural perturbations originating from the loss of the Arg^{106} side chain point to a role of the L2 loop in stabilizing the closed conformation of the L7 loop. Despite the increased exposure of the R106G active site, no abnormal reaction of PEP with water was observed, ruling out the hypothesis that the primary function of the L7 loop is to shield the active site from bulk solvent during the condensation reaction. However, the R106G enzyme displays several kinetic abnormalities on both the substrate side (smaller K_m^{PEP}, larger K_i^{A5P} and K_m^{A5P}) and the product side (smaller K_i^{Pi} and K_i^{KDO8P}) of the reaction. As a consequence, the mutant enzyme is less severely inhibited by A5P and more severely inhibited by P_i and KDO8P. Simulations of the flux of KDO8P synthesis under metabolic steady-state conditions (constant concentration of reactants and products over time) suggest that in vivo R106G is expected to perform optimally in a narrower range of substrate and product concentrations than the wild-type enzyme.

3-Deoxy-D-*manno*-octulosonate 8-phosphate synthase (KDO8PS, EC 2.5.1.55) catalyzes the irreversible condensation of phosphoenolpyruvate (PEP)[1] and arabinose 5-phosphate (A5P) to form KDO8P and inorganic phosphate (Figure 1) (*1*−*5*). This reaction is the first step in the biosynthesis of 3-deoxy-D-*manno*-octulosonate (KDO), an essential component of the lipopolysaccharide of all Gram-negative bacteria (*6*, *7*).

There are two types of KDO8PSs, distinguished by their requirement for divalent metals (Class II) or lack thereof (Class I) (*8*). In previous studies, we have determined the crystal structure of KDO8PS from the hyperthermophile *Aquifex aeolicus* (a Class II KDO8PS) in complex with Cd^{2+} (*2*, *3*), the metal conferring the highest activity in vitro (*9*). All known KDO8PSs, with the exception of the *Arabidopsis thaliana* enzyme (*10*), are tetramers. However, the asymmetric unit of *A. aeolicus* KDO8PS crystals contains only two subunits, named here A and B. PEP binds to both subunits, but A5P binds only to subunit A (*2*). Moreover, if crystal symmetry is applied to generate the tetramer, it is apparent that the active sites in which A5P binds are located on the same face of the enzyme (*2*). Based on this observation and the assumption that, at some point, both faces of the enzyme may participate in catalysis, it has been proposed that *A. aeolicus* KDO8PS may represent an interesting case of "alternating face" catalysis (*2*).

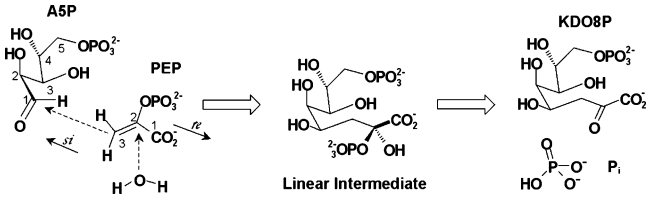

FIGURE 1: Biosynthesis of KDO8P from A5P and PEP. Attack by water onto $C2^{PEP}$ and by $C3^{PEP}$ onto $C1^{A5P}$ leads to a linear intermediate that decays into P_i and KDO8P.

Three long loops, L2, L7, and L8, control access to the active site. In the substrate-free enzyme and when only PEP or A5P binds, residues 190−200 of the L7 loop are disordered (*2*, *3*) (Figure 2A). However, when both substrates bind, the L7 loop is ordered and isolates the active site from the external environment (Figure 2B). It has been proposed that Arg^{106} of *A. aeolicus* KDO8PS, a residue conserved in all KDO8PSs, might be involved in regulating the opening and closing of the L7 loop in different subunits (*2*). The structural basis for this hypothesis is the somewhat unusual

[†] This research was supported by U.S. Public Health Service Grants GM69840 to D.L.G.

[‡] The structure-factor amplitudes and refined coordinates of substrate-free R106G, R106G with PEP, and PEP *plus* A5P, were deposited in the Protein Data Bank (entries 1T99, 1T96, 1T8X, respectively).

[§] These authors have contributed equally to the work.

* Corresponding author: Domenico L. Gatti, Department of Biochemistry and Molecular Biology, Wayne State University School of Medicine, Detroit, MI 48201. Tel, (313) 577-0620; fax, (313) 577-2765; e-mail, mimo@boatman.med.wayne.edu.

[1] Abbreviations: KDO, 3-deoxy-D-*manno*-octulosonate; KDO8P, 3-deoxy-D-*manno*-octulosonate 8-phosphate; KDO8PS. 3-deoxy-D-*manno*-octulosonate 8-phosphate synthase; PEP, phosphoenolpyruvate; A5P, arabinose 5-phosphate; 2-PGA, 2-phosphoglycerate; DSS, 2,2-dimethylsilapentane-5-sulfonic acid; DDM, difference-distance matrix; EDDM, error-scaled difference-distance matrix; SSR, sum of squared residuals; rmsd, root-mean-square deviation; H, helix; S, strand; L, loop.

10.1021/bi051095q CCC: $30.25
Published on Web 08/26/2005

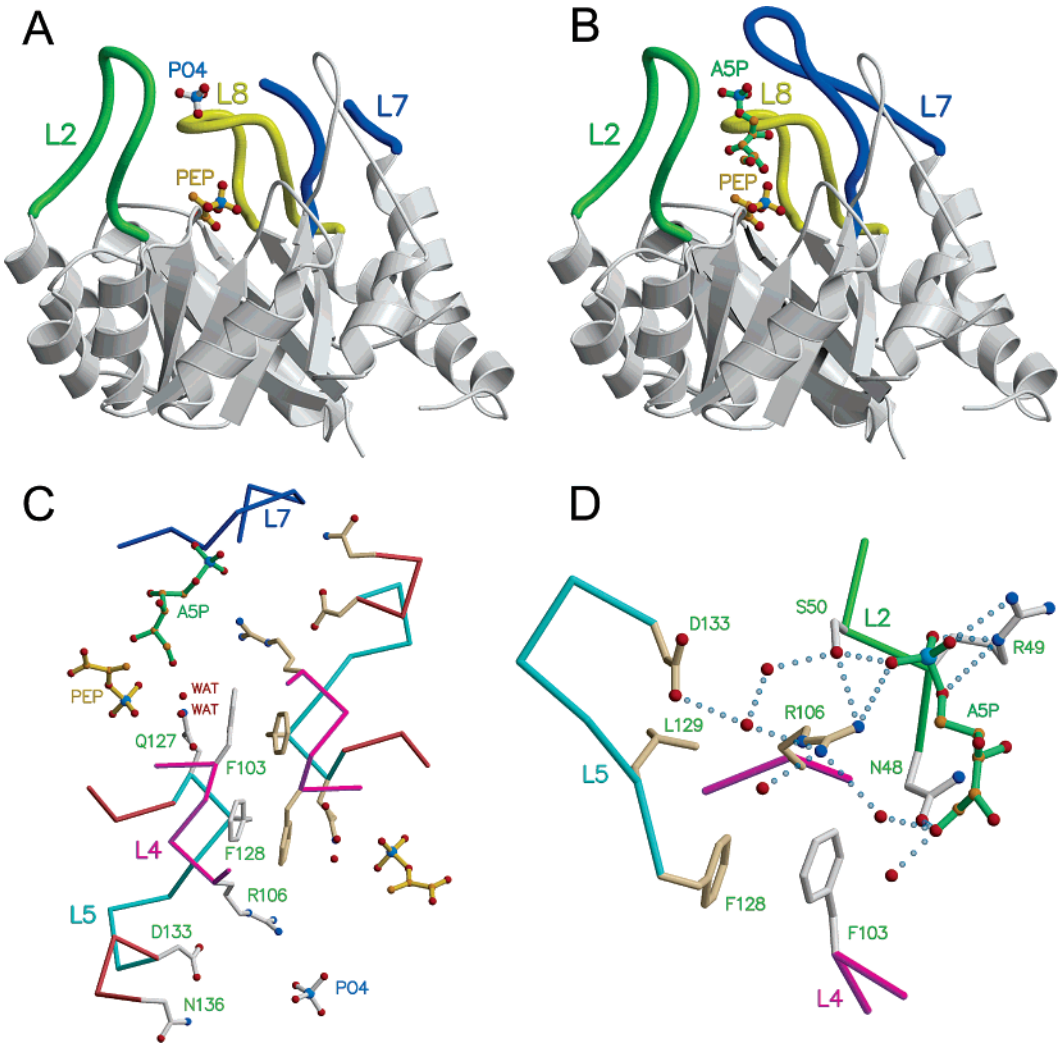

FIGURE 2: Conformational changes in wild-type KDO8PS.The three loops that seal the barrel cavity in *A. aeolicus* KDO8PS are shown as thick tubes with different colors: L2, green; L7, blue; and L8, yellow. The L7 loop is disordered when PEP is bound (panel A, PDB entry 1FWS), but ordered and closed when both PEP and A5P bind (panel B, PDB entry 1FWW). This conformation of the L7 loop is particularly evident in the two adjacent subunits of the enzyme shown in panel C. In one subunit, A5P is bound, and the L7 loop is ordered. In the other subunit, a phosphate ion is bound instead of A5P, and the L7 loop is not visible (disordered). Notice how the side chain of Arg^{106} crosses over from one subunit into the active site of the other subunit (panel C). The stacking of phenyl rings from the L5 (cyan) and L4 (magenta) loops at the interface between adjacent subunits provides part of the pocket for Arg^{106} side chain (panel D). In both panels C and D, side chains originating from different subunits are colored gray and beige, respectively. Waters are represented as red spheres, hydrogen bonds as dashed lines.

position of Arg^{106}, whose side chain extends from one subunit into the active site of another subunit (Figure 2C). More specifically, Arg^{106} from one subunit is sandwiched between the side chains of Phe^{128}, Leu^{129}, and Asp^{133} (loop L5) from the same subunit and the backbone and side chains of Asn^{48}, Arg^{49}, Ser^{50} (loop L2), and Phe^{103} (loop L4) from the other subunit (Figure 2C,D). Here, we report that the $Arg^{106} \rightarrow$ Gly substitution impairs the L7 loop closure, thus, providing a unique opportunity to study the function of this loop.

EXPERIMENTAL PROCEDURES

Structure Determination and Refinement. A. aeolicus KDO8PS was produced in *Escherichia coli* from plasmid pet28a/*kdsa*, which was derived from plasmid pet28a (Novagen) by inserting the *A. aeolicus KDSA* gene in frame with the ATG of the vector *Nco I* site. Plasmid pet28a/*kdsaR106G* encoding the mutant R106G protein was derived from the wild-type-encoding plasmid by replacing the Arg codon AGG with the Gly codon GGG using the Quick-Change (Stratagene) mutagenesis system. Both the wild-type and mutant proteins were purified by a modification of the procedure described by Duewel (*11*). The main difference in the new purification scheme is that, after breaking the cells (~50 mL) with two passes through a French press at 4 °C, the initial heat step is carried out in a 100 mL glass cylinder (with stirring) submersed in a 1 L beaker containing stirring water at 80 °C. The temperature ramps up to 80 °C in the cylinder in less than 3 min, after which the sample is incubated under stirring at 80 °C for an additional 10 min. The cylinder is rapidly transferred to a beaker with stirring ice−water until its content, still under stirring, cools to 2 °C (~3min), and then placed in ice for additional 10 min. After removal by ultracentrifugation of the denatured protein, the clear supernatant derived from 1 L of the original culture is loaded onto 3 BioRad Econo-Pac High-Q cartridges (each 5 mL bed volume) assembled in series, equilibrated with 20 mM Tris-Cl (pH 7.5), and eluted with a linear gradient (120 mL) from 0 to 1 M NaCl. Fractions containing recombinant

Table 1: X-ray Data Collection and Refinement Statistics[a]

	R106G	+ PEP	+ PEP + A5P
Data Collection			
resolution range (Å)	42−1.85 (1.97−1.85)	41−1.85 (1.97−1.85)	54−1.8 (1.87−1.8)
unique reflections	56 873 (4771)	55 179 (3994)	60 408 (4268)
⟨redundancy⟩	10.3 (3.8)	3.7 (1.3)	9.2 (1.85)
completeness (%)	92.8 (71.2)	89.6 (59.8)	94.3 (62.4)
$\langle I\rangle/\sigma\langle I\rangle$	4.7 (2.1)	5.2 (2.1)	4.5 (2.2)
R_{merge}[b] (%)	9.3 (35.9)	9.4 (34.4)	9.5 (34.7)
Refinement			
PDB entry	1T99	1T96	1T8X
R_{cryst}[c] (%)	20.8	20.4	19.7
R_{free} (%)	24.5	24.6	24.2
amino acids	509	509	511
water molecules	325	486	441
model $\langle B\rangle$ (Å^2)	37.7	29.5	34.3
rmsd bond lengths (Å)	0.009	0.009	0.005
rmsd bond angles (deg)	1.5	1.5	1.5
rmsd dihedral (deg)	22.7	22.7	22.6
rmsd impropers (deg)	0.89	0.90	0.92

[a] Each data set was collected from a single crystal at 100 K. [b] $R_{merge} = \sum_h\sum_i|I(h)_i - \langle I(h)\rangle|/\sum_h\sum_i I(h)_i$, where $I(h)_i$ is the ith measurement. [c] $R_{cryst} = \sum|F_{obs} - F_{calc}|/\sum|F_{obs}|$. R_{free} was calculated on 10% of the data omitted from refinement. Numbers in parentheses refer to the highest resolution shell.

KDO8PS (already approximately 90% pure at this stage) are loaded directly onto 3 BioRad Econo-Pac CHT-II (ceramic hydroxyapatite) cartridges (each 5 mL bed volume) equilibrated with 20 mM Tris-Cl (pH 7.5), and eluted with a linear gradient (60 mL) from 0 to 400 mM K-phosphate (pH 7.5). Fractions containing the pure enzyme are dialyzed for 24 h against 20 mM Tris-Cl (pH 7.5) and 50 μM $CdCl_2$, with changes every 4−8 h, concentrated to ∼40 mg/mL, and flash-frozen in liquid nitrogen.

Crystals of *A. aeolicus* KDO8PS were obtained as described previously (*2*, *11*). Crystals belong to space group $P3_121$, with unit cell dimensions $a = b \cong 84.3$ Å, $c \cong 159.5$ Å, and diffract to ∼1.8 Å. Oscillation data were collected at 100 K with an HTC image plate detector at the Cu Kα wavelength (Table 1) and processed with HKL (*12*). As crystals of the mutant enzyme are highly isomorphous to those of the wild-type, standard crystallographic refinement starting from the wild-type model (PDB entry 1FXP (*2*)) was sufficient to determine the structure. This was carried out with CNS v. 1.1 using cross-validated maximum likelihood as the target function (*13*). Water molecules were added to the model by means of several cycles of the automated routine for water identification available in CNS, each cycle being followed by a visual examination of the model.

Error-Scaled Difference-Distance Matrices. In a distance matrix, the differences between the coordinates of each Cα of a protein and every other Cα of the same protein are used to build a density plot in which residues close in space are represented as a point of high density. In a difference-distance matrix (DDM), the distance matrix of a first structure is subtracted from the distance matrix of a second structure, so that each element of the DDM has the form $\Delta_{ij}^{ab} = D_{ij}^{a} - D_{ij}^{b}$. However, as the elements of a DDM are small differences between large numbers with errors and these errors vary in different structures, DDMs are typically very noisy. To overcome this problem, we have used the program ESCET (*14*, *15*) to place the uncertainties of atomic coordinates in different structures on the same scale. In ESCET, the value for the standard radial coordinate uncertainty σ_r of any atom of the structure having a B factor equal to the average B is estimated using the DPI (Diffraction Precision Indicator) method (*16*). The estimated positional error $\sigma_{r,i}$ of the i atom with B factor B_i is derived from the linear relationship $\sigma_{r,i} = \sigma_r\ B_i/B_{avg}$ between coordinate uncertainty and B factor. The error of the Δ_{ij}^{ab} element of a DDM can then be calculated as $\sigma(\Delta_{ij}^{ab}) = [(\sigma_{r,i}^{a})^2 + (\sigma_{r,j}^{a})^2 + (\sigma_{r,i}^{b})^2 + (\sigma_{r,j}^{b})^2]^{1/2}$. Finally, the elements of the DDM are normalized by their error according to $E_{ij}^{ab} = \Delta_{ij}^{ab}/\sigma(\Delta_{ij}^{ab})$. This results in an error-scaled difference-distance matrix (EDDM), in which each element is a multiple of $\sigma(\Delta_{ij}^{ab})$. Table 2 shows some statistics for the $\sigma_{r,i}$ of the Cα atoms of the structures compared in this study.

Table 2: Estimated Positional Errors in the Structures of the Wild-Type and R106G Enzymes[a]

	estimated positional error ($\sigma_{r,i}$) in Å for 250 Cα atoms			
	mean	σ	min	max
WT (subunit A)	0.121	0.025	0.084	0.199
WT (subunit B)	0.139	0.035	0.089	0.248
WT + PEP (subunit A)	0.112	0.025	0.069	0.233
WT + PEP (subunit B)	0.128	0.031	0.074	0.235
WT + PEP, A5P (subunit A)	0.116	0.023	0.081	0.207
WT + PEP, A5P (subunit B)	0.131	0.028	0.087	0.225
R106G (subunit A)	0.086	0.022	0.058	0.152
R106G (subunit B)	0.100	0.024	0.059	0.172
R106G + PEP (subunit A)	0.093	0.029	0.050	0.203
R106G + PEP (subunit B)	0.108	0.030	0.060	0.224
R106G + PEP, A5P (subunit A)	0.078	0.021	0.051	0.142
R106G + PEP, A5P (subunit B)	0.089	0.021	0.051	0.170

[a] Coordinates for the wild-type structures are from PDB entries 1FXP, 1FWS, and 1FWW (*2*).

^{31}P NMR of KDO8P Synthesis in the R106G Enzyme. Product formation in the R106G enzyme was followed by ^{31}P NMR. Each 1D NMR spectrum was collected at 10 °C by accumulating the signal for 20 min over a range of 20 ppm in a Varian Mercury 400 MHz NMR spectrometer equipped with a 5 mm autotunable broadband Varian probe. Spectra were referenced indirectly to a 2,2-dimethylsilapentane-5-sulfonic acid (DSS) external control. Pyruvate formed during the course of the reaction was assayed following the oxidation of NADH associated with the reduction of pyruvate to lactate by lactate dehydrogenase (*17*).

Nonlinear Regression Analysis of Reaction Progress Curves. Rate constants for the reaction catalyzed by KDO8PS were determined by nonlinear regression analysis (*18*) of multiple progress curves of PEP consumption at 40 °C. This temperature was found to be a good compromise between achieving sufficient activation of the thermophilic KDO8PS and limiting the nonenzymatic hydrolysis of PEP at high temperature. The curves were recorded at 232 nm (ϵ^{PEP} = 2840 M^{-1} cm^{-1}) when the enzyme (2 μM) was added to a solution containing 100 mM Tris-acetate (pH 7.5), 50 μM $CdCl_2$, and several different concentrations and molar ratios of PEP, A5P, and P_i (Table 3). On the basis of previous kinetic analyses of *E. coli* KDO8PS (*19*−*23*), KDO8P synthesis was treated as a Bi−Bi ordered reaction in which PEP binds before A5P (*19*) and inorganic phosphate leaves before KDO8P. A global fit of all the progress curves with a unique set of rate constants was obtained using the program Dynafit (*24*). The quality of the nonlinear regression analysis

Table 3: Initial Concentrations of Substrates and Products in 19 Reaction Progress Curves Catalyzed by the Wild-Type and R106G Enzymes[a]

	wild-type			R106G		
progress curve	PEP (μM)	A5P (μM)	P_i (μM)	PEP (μM)	A5P (μM)	P_i (μM)
1	102	202	0	107	198	0
2	106	303	0	105	296	0
3	197	302	0	201	293	0
4	135	588	0	153	490	0
5	296	596	0	295	585	0
6	434	596	0	437	585	0
7	247	94	0	304	121	0
8	294	195	0	275	166	0
9	386	195	0	368	210	0
10	482	91	0	454	99	0
11	384	228	0	394	247	0
12	483	278	0	482	297	0
13	586	421	0	569	427	0
14	441	98	600	484	97	600
15	488	99	900	487	102	900
16	105	202	300	98	198	300
17	105	203	600	108	198	600
18	479	99	2000	496	110	2000
19	256	346	4000	105	195	4000

[a] The enzyme concentration in each experiment was 2 μM.

was assessed on the basis of the sum of the squared residuals (SSR) between the simulated and the experimental progress curves, the magnitude of the standard error associated with each refined parameter, and the spread of errors among all parameters. The steady-state rate equation for KDO8P synthesis was derived by application of the King−Altman method (*25*−*27*). Kinetic constants were calculated by substituting the rate constants into the rate equation according to Cleland's rules (*28*). The standard errors of the kinetic constants were calculated from the standard errors of the rate constants by traditional rules of error propagation.

The steady-state concentrations of the reaction species and the flux of KDO8P synthesis under conditions in which the concentrations of substrates and products remain constant over time were calculated from the rate constants using the program Gepasi (*29*). Gepasi accomplishes this task by setting the differential equations that describe the time evolution of the system to zero. The resulting system of nonlinear algebraic equations is solved using the LSODA (Livermore Solver of Ordinary Differential Equations) routine (*30*).

RESULTS

Structure of the R106G Enzyme. We have determined the crystal structures of the R106G mutant without substrate, with PEP, and with PEP *plus* A5P bound (Table 1). The most dramatic structural difference between wild-type and mutant is in the L7 loop. In the wild-type, this loop is disordered when either PEP or A5P is bound, but becomes ordered and seals the active site when A5P and PEP bind together (*2*) (Figures 2 and 3). Similarly to the wild-type, in crystals of R106G incubated with 5 mM PEP and 10 mM A5P, PEP binds in both subunits, A5P binds in subunit A only, and a phosphate ion occupies the position of the phosphate moiety of A5P in subunit B. However, in R106G, the L7 loop is disordered and the active site is open even in the subunit where both substrates bind (Figure 3). Other

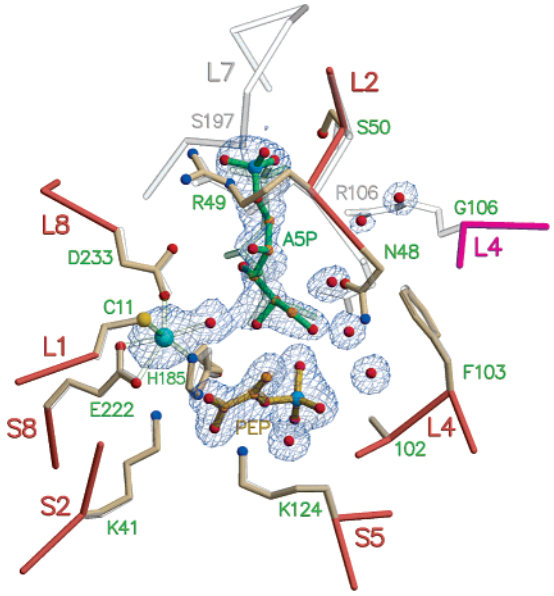

FIGURE 3: PEP and A5P binding in the wild-type and R106G enzymes. The Cα trace of R106G is shown with salmon (subunit A) and magenta (subunit B) bonds. Cd^{2+} coordination is shown as transparent bonds. Side chains are shown with beige (R106G) and transparent (wild-type) bonds. Note how the Arg^{106} side chain is replaced by water molecules in R106G. The L2 loop is shifted in R106G, which contrasts with the essentially unchanged position of the other elements of the active site. The L7 loop is visible (ordered) only in the wild-type (transparent bonds). PEP is unchanged in the wild-type (transparent bond) and in R106G (gold bonds), while A5P displays two slightly different conformations in the wild-type (transparent bonds) and in R106G (green bonds). A σA-weighted omit map around PEP and A5P is contoured at 1 σ. Nitrogen, blue; oxygen, red; carbon, orange; sulfur, yellow; phosphorus, pale blue; and cadmium, cyan.

differences are a direct consequence of the mutation; for example, the side chain of Arg^{106} is replaced by one or more water molecules (Figure 3). Furthermore, when the mutant and wild-type structures are superimposed, small displacements of the residues surrounding Arg^{106} are recognized. The most significant among these changes in either subunit A or B occurs in the region corresponding to residues 45−55 (Figure 3, see also the EDDMs of Figure 4). These residues, many of which line the active site cavity and provide most of the protein interactions with A5P (e.g., Asn^{48}, Arg^{49}, and Ser^{50}), belong to the long L2 loop connecting the β-strand and α-helix of the 2nd β/α unit of the barrel. Surprisingly, in the R106G mutant, residues 45−55 of the L2 loop move slightly away from the cavity left by the loss of Arg^{106} rather than trying to fill it (Figure 3). This is perhaps due to the loss of hydrogen bonds of the guanidinium group of Arg^{106} with the side chain of Ser^{50} (Figure 2), and also with the backbone of both Ser^{50} and Asn^{48} (not shown). As a consequence of the partial opening of the L2 loop, the A5P position is more peripheral, such that the distance (at their closest approach) between the phosphate moieties of PEP and A5P is 11.14 versus 10.32 Å in the wild-type (Figure 3). The electron density of A5P is well-defined and shows the *re* side of the aldehyde moiety facing the *si* side of $C2^{PEP}$ (Figure 3), in agreement with previous stereochemical studies (*22*, *23*, *31*). However the positions of the C3−OH and C4−OH are different from the wild-type (Figure 3), confirming earlier observations of conformational flexibility in A5P (*2*). The same positional changes of the L2 loop observed in the

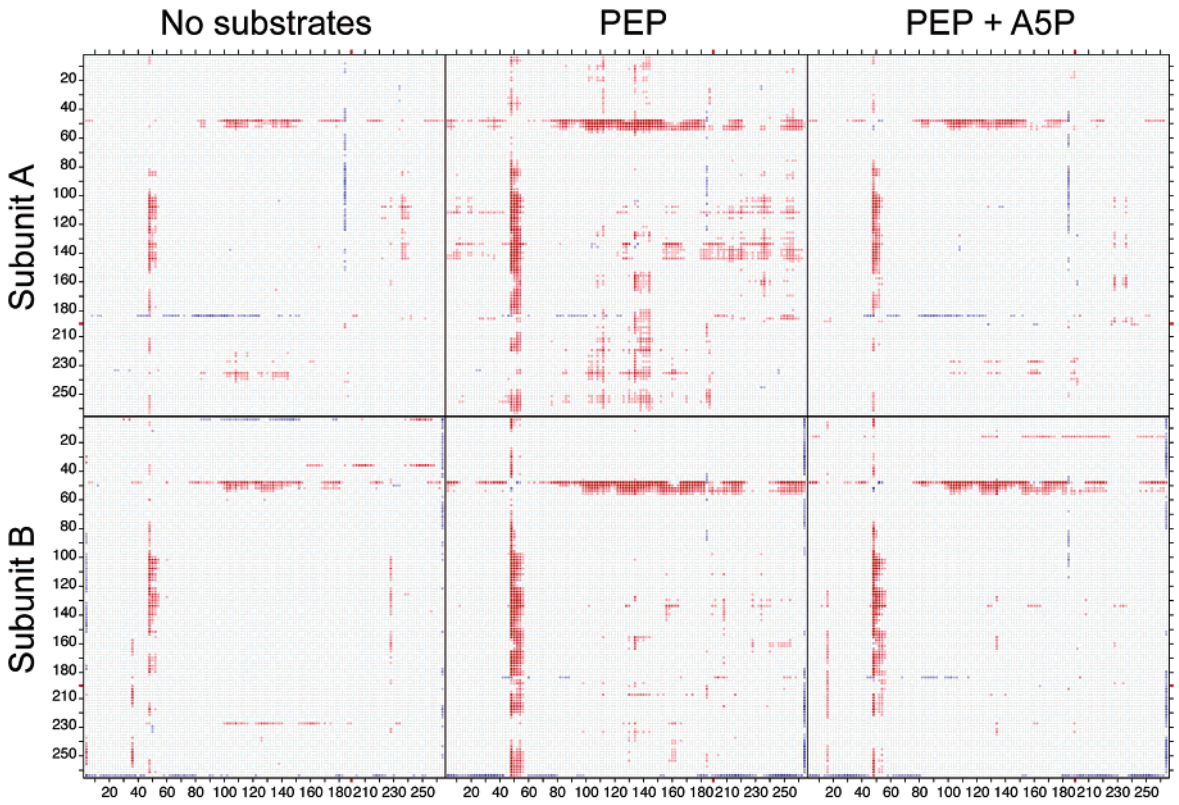

FIGURE 4: Error-scaled difference-distance matrices (EDDM) between wild-type and R106G. EDDMs for the A and B subunits are shown in the upper and lower panels, respectively. Positive and negative differences are shown as red (expansion in the length of the corresponding interatomic vector) and blue (contraction in the length of the corresponding interatomic vector), respectively. Only differences between 1.5 and 3.6 $\sigma\Delta_{ij}^{ab}$ are displayed. The L7 loop region encompassing residues 189−200 was not included in the computation of the EDDMs (a red tick marks the position of the excluded fragment) because the coordinates for this region are known only in the wild-type. Therefore, there is no special feature in the EDDMs reporting the different conformations of the L7 loop in the wild-type and in R106G

presence of PEP *plus* A5P, occur also in the absence of any substrates or in the presence of only 5 mM PEP (Figure 4), suggesting they are indeed a primary structural consequence of the R106G substitution. In the presence of PEP, some additional motion of the L4 loop (residues 100−140) is observed in the mutant A subunit (center top EDDM of Figure 4).

The purified R106G enzyme, regardless of the presence of one or both substrates, has spectral properties comparable to those of the wild-type (data not shown), suggesting that there are no significant changes in the coordination of the active site metal (Cd^{2+}). The X-ray structure shows that Cd^{2+} retains the usual octahedral coordination with Cys^{11}, His^{185}, Glu^{222}, Asp^{233}, and a water molecule (Figure 3), although, in subunit A only, the imidazole ring of His^{185} is slightly rotated with respect to the wild-type (Figure 3; see also the negative line of pixels corresponding to His^{185} in the top panels of Figure 4).

Enzymatic Activity of the R106G Enzyme. Early studies of *E. coli* KDO8PS by Hedstrom (*5*), Kohen (*19*), and Baasov (*20*, *21*) have established that KDO8P synthesis is irreversible, that PEP binds before A5P, and that inorganic phosphate leaves the enzyme before KDO8P. This order of substrate binding and product release is supported by the observations that ribose 5-phosphate is competitive with respect to A5P and uncompetitive with respect to PEP and that KDO8P is competitive with respect to PEP (thereby KDO8P and PEP bind to the same enzyme form) and uncompetitive with respect to A5P. Altogether, these findings are consistent with a traditional Bi−Bi sequential mechanism

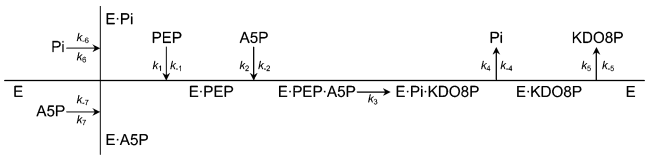

FIGURE 5: Kinetic model of KDO8P synthesis. Noncovalent complexes are represented with dots.

A + B → P + Q, in which A = PEP, B = A5P, P = P_i, and Q = KDO8P.

The order of substrate binding established by the kinetic studies finds a structural explanation in the fact that the active site is shaped as a funnel, with PEP sitting at the bottom and A5P binding above it, near the opening to the bulk solvent (Figures 2 and 3). As PEP cannot enter the active site if A5P is bound, A5P is expected to behave both as a substrate (when it binds sequentially to PEP) and as a dead-end inhibitor of the enzyme (when it binds independently from PEP, as shown in the structure of *A. aeolicus* KDO8PS in complex with A5P (*2*)). Also, the structure of substrate-free enzyme shows inorganic phosphate bound at the sites of the phosphate moieties of PEP and A5P (*2*). Therefore, inorganic phosphate may act as a competitive inhibitor with respect to PEP and A5P. This is in addition to the fact that phosphate, as the first product released in a Bi−Bi reaction, is expected to act as an uncompetitive inhibitor with respect to both substrates (*19*, *26*). A model for the catalytic cycle of KDO8PS including the aforementioned features is shown in Figure 5. In this model, the irreversible step of the reaction (*5*) is assumed to be the conversion of bound substrates into

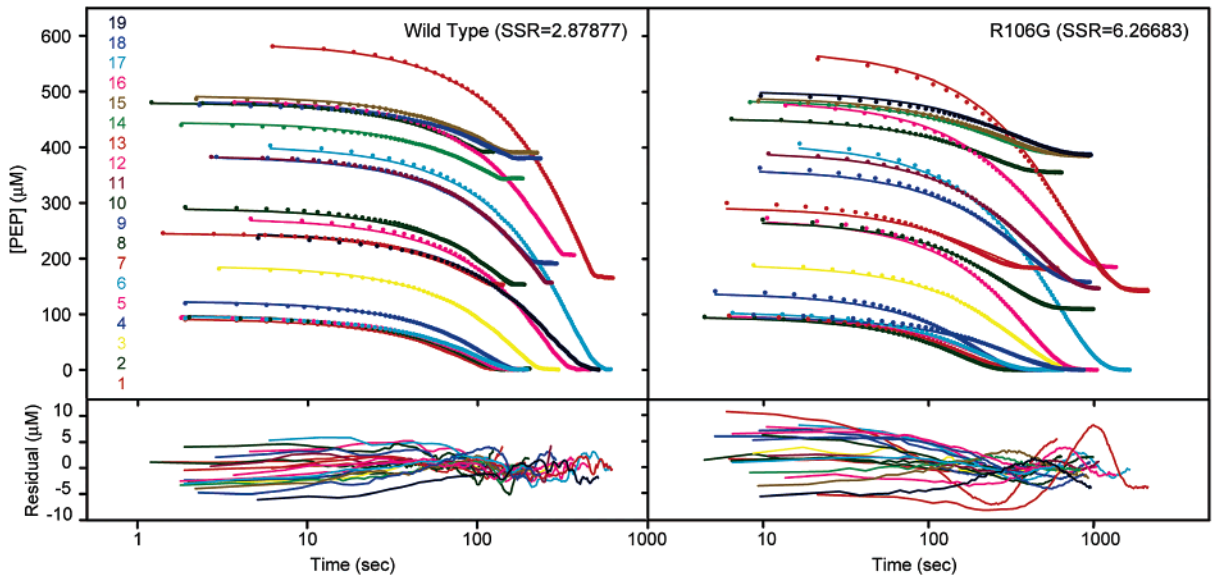

FIGURE 6: Progress curves of PEP consumption by the wild-type and R106G enzymes. The spectrophotometric signal collected at 232 nm is already converted into PEP concentrations ($\epsilon^{PEP} = 2840\ M^{-1}\ cm^{-1}$). Experimental points and simulated curves are shown as filled circles and solid lines, respectively. To display the quality of the fit in both short and long traces, a log scale is used for the time axis. Curve numbers are the same as in Table 3. The residuals between the simulated and experimental curves are shown in the lower panels. SSR values (divided by the number of contributing points) for the two global fits are shown in parentheses.

bound products. We have used nonlinear regression analysis as implemented in the program Dynafit (*24*) to test the potential of this model to simulate experimental progress curves in which KDO8P synthesis is monitored by following the decrease in absorbance at 232 nm due to the stoichiometric disappearance of PEP (see Experimental Procedures). Reactions were carried out at 40 °C by mixing 2 μM KDO8PS with several different concentrations and molar ratios of PEP, A5P, and P_i (Table 3). A total of 19 curves were analyzed globally (simultaneous fit of all the progress curves) for both the wild-type and R106G. The principle of statistical cross-validation (*32*, *33*) was adopted to avoid overfitting the set of progress curves with too many parameters. For this purpose, in a preliminary analysis, three progress curves were randomly selected out of the 19 and set aside as a "free set"; the remaining 16 curves were included in a "working set" and fitted globally. The refined parameters from the working set were then used in the calculation of the residual for the free set. The parameters that, when included in the model, decreased the difference between the working and free set residuals were retained, while those that increased the difference were discarded even if the working set residual became smaller. For example, the model shown in Figure 5 was tested against an alternative model (not shown) that included parameters representing the isomerization of the free and liganded forms of the enzyme between a state in which the L7 loop is open and a state in which it is closed. As a result of the cross-validation analysis, the parameters describing A5P as a substrate inhibitor and P_i as a competitive inhibitor were retained in the final model, while those describing the enzyme isomerization between open and closed forms were rejected. In the end, optimal global fit of the set of all 19 progress curves for both the wild-type and R106G was based on the refinement of a total of 11 rate constants and 19 protein concentrations. Since each progress curve consists of 100 points (for a total of 1900 points), the set of 30 solutions is overdetermined. The experimental and simulated progress curves for both the wild-type and R106G are shown in Figure 6. The refined values of the 11 rate constants for both enzymes and the associated standard errors are shown in Table 4. The rate equation for this model was derived by application of the King−Altman method (*25*−*27*); its numerator and denominator coefficients are shown in Table 5. Kinetic constants were calculated from the rate constants according to Cleland's rules, which define k_{cat}, K_m's, and K_i's as ratios between different coefficients in the rate equation (*26*, *28*). The standard errors of the kinetic constants were calculated from the standard errors of the rate constants by error propagation.

Table 4: Rate Constants (± Standard Errors) for KDO8P Synthesis in the Wild-Type and R106G Enzymes[a]

reaction step	rate constants	wild-type	R106G
E + PEP ⇔ E·PEP	k_1	10.98 ± 0.67	11.64 ± 1.90
	k_{-1}	4.86 ± 0.62	0.43 ± 0.04
E·PEP + A5P ⇔ E·PEP·A5P	k_2	8.23 ± 1.00	10.47 ± 1.10
	k_{-2}	60.21 ± 8.00	789 ± 82.00
E·PEP·A5P ⇒ E·Pi·KDO8P	k_3	0.53 ± 6.4 × 10^{-3}	0.42 ± 0.01
E·Pi·KDO8P ⇔ E·KDO8P + P_i	k_4	30950 ± 5800	7337 ± 810
	k_{-4}	8.06 ± 1.10	9.25 ± 1.10
E·KDO8P ⇔ E + KDO8P	k_5	5.33 ± 0.63	1.36 ± 0.10
	k_{-5}	4.32 ± 0.50	5.30 ± 0.93
E + P_i ⇔ E·Pi	k_6	4.08 ± 0.73	24.61 ± 4.90
	k_{-6}	66.53 ± 9.80	26860 ± 3400
E + A5P ⇔ E·A5P	$k_7 = k_2$	8.23 ± 1.00	10.47 ± 1.10
	$k_{-7} = k_{-2}$	60.21 ± 8.00	789 ± 82.00

[a] Noncovalent complexes are represented with a dot symbol. First-order rate constants are in units of s^{-1}. Second-order rate constants are in units of $\mu M^{-1}\ s^{-1}$.

Analysis of Table 4 suggests that only six rate constants (k_{-1}, k_{-2}, k_4, k_5, k_6, and k_{-6},) are significantly different in the wild-type and in R106G. Changes in the *on* and *off* rate for PEP (k_1, k_{-1}) in R106G with respect to the wild-type produce a 10-fold decrease in the K_d for PEP, which might reflect an easier access by this substrate to the active site as a consequence of the prevalent open state of the L7 loop.

Table 5: Rate Equation for the Kinetic Model Shown in Figure 5

$$v = \boldsymbol{N}/\boldsymbol{D}$$
$$\boldsymbol{N} = n_1[\mathrm{PEP}][\mathrm{A5P}]$$
$$\boldsymbol{D} = d_1[\mathrm{A5P}][\mathrm{Pi}][\mathrm{KDO8P}] + d_2[\mathrm{PEP}][\mathrm{A5P}][\mathrm{Pi}] + d_3[\mathrm{Pi}][\mathrm{KDO8P}] + d_4[\mathrm{A5P}][\mathrm{KDO8P}] + d_5[\mathrm{A5P}][\mathrm{Pi}] + d_6[\mathrm{A5P}]^2 + d_7[\mathrm{PEP}][\mathrm{A5P}] + d_8[\mathrm{KDO8P}] + d_9[\mathrm{Pi}] + d_{10}[\mathrm{A5P}] + d_{11}[\mathrm{PEP}] + d_{12}$$
$$n_1 = k_1k_2k_3k_4k_5k_{-6}k_{-7}$$
$$d_1 = k_2k_3k_{-4}k_{-5}k_{-6}k_{-7}$$
$$d_2 = k_1k_2k_3k_{-4}k_{-6}k_{-7}$$
$$d_3 = k_{-1}k_{-2}k_{-4}k_{-5}k_{-6}k_{-7} + k_{-1}k_3k_{-4}k_{-5}k_{-6}k_{-7}$$
$$d_4 = k_2k_3k_4k_{-5}k_{-6}k_{-7}$$
$$d_5 = k_2k_3k_4k_5k_6k_{-7}$$
$$d_6 = k_2k_3k_4k_5k_{-6}k_7$$
$$d_7 = k_1k_2k_4k_5k_{-6}k_{-7} + k_1k_2k_3k_5k_{-6}k_{-7} + k_1k_2k_3k_4k_{-6}k_{-7}$$
$$d_8 = k_{-1}k_{-2}k_4k_{-5}k_{-6}k_{-7} + k_{-1}k_3k_4k_{-5}k_{-6}k_{-7}$$
$$d_9 = k_{-1}k_{-2}k_4k_5k_6k_{-7} + k_{-1}k_3k_4k_5k_6k_{-7}$$
$$d_{10} = k_2k_3k_4k_5k_{-6}k_{-7} + k_{-1}k_{-2}k_4k_5k_{-6}k_7 + k_{-1}k_3k_4k_5k_{-6}k_7$$
$$d_{11} = k_1k_{-2}k_4k_5k_{-6}k_{-7} + k_1k_3k_4k_5k_{-6}k_{-7}$$
$$d_{12} = k_{-1}k_{-2}k_4k_5k_{-6}k_{-7} + k_{-1}k_3k_4k_5k_{-6}k_{-7}$$

Table 6: Kinetic Constants (± Standard Errors) for KDO8P Synthesis in the Wild-Type and R106G Enzymes[a]

rate equation coefficients	kinetic constants	wild-type	R106G
n_1/d_7	k_{cat}	0.48 ± 0.21	0.32 ± 0.12
d_{10}/d_7	K_m^{PEP}	0.45 ± 0.20	0.06 ± 0.02
d_{11}/d_7	K_m^{A5P}	6.71 ± 2.98	57.7 ± 21.1
k_{-1}/k_1	K_d^{PEP}	0.44 ± 0.06	0.04 ± 7e^{-3}
k_{-2}/k_2	$K_d^{A5P} \equiv K_i^{A5P}$	7.31 ± 1.32	75.4 ± 11.1
k_4/k_{-4}	$K_d^{Pi\text{-}1}$	3838 ± 890	793 ± 129
d_7/d_2	$K_i^{Pi\text{-}1}$	42305 ± 17223	3373 ± 1223
k_5/k_{-5}	K_d^{KDO8P}	1.23 ± 0.21	0.26 ± 0.05
d_{10}/d_4	K_i^{KDO8P}	12.6 ± 5.6	0.52 ± 0.17
k_{-8}/k_8	$K_d^{Pi\text{-}2}$	16.3 ± 3.8	1091 ± 258
d_{10}/d_5	$K_i^{Pi\text{-}2}$	166 ± 76	2215 ± 734

[a] The k_{cat} is in units of s^{-1}; all other kinetic constants are in units of μM.

Changes in the *on* and *off* rate for A5P (k_2, k_{-2}) are responsible for a 10-fold increase in the K_d (as substrate) ≡ K_i (as competitive inhibitor) for A5P in the mutant enzyme. This finding is consistent with the structural observation that the guanidinium moiety of Arg^{106} forms a weak salt bridge with the phosphate moiety of A5P (3.5 Å at their closest approach; Figure 2). Values of $\Delta\Delta G_{A5P}$ of 1.45 and 1.59 kcal/mol are obtained, respectively, for the effect of the R106G substitution on the relative free energy of bound A5P according to $\Delta\Delta G = -RT\ln(K_d^{WT}/K_d^{R106G})$, or $\Delta\Delta G = -RT\ln[(k_{cat}/K_m^{R106G})/(k_{cat}/K_m^{WT})]$. These values are well within the range of ligand-binding energies provided by salt bridges in proteins (*34*). An 8-fold increase of K_m^{A5P} is also observed in R106G (Table 6).

The *on* and *off* rates for P_i (k_{-4}, k_4) and KDO8P (k_{-5}, k_5) on the product side of the reaction, define the dissociation constants $K_d^{Pi\text{-}1}$ and K_d^{KDO8P} (Table 6), which are approximately 5 times smaller in the mutant. The inhibition constants $K_i^{Pi\text{-}1}$ and K_i^{KDO8P} (Table 6) are derived from the rate equation coefficients of Table 5 and, thus, reflect more global changes in the rate constants of all the steps. These inhibition constants refer to the fact that P_i (uncompetitively) and KDO8P (competitively with respect to PEP, uncompetitively with respect to A5P) behave as product inhibitors (*26*). In R106G, $K_i^{Pi\text{-}1}$ and K_i^{KDO8P} are 13 and 24 times smaller than in the wild-type, respectively. Thus, both products bind better and are stronger product inhibitors in the mutant than in the wild-type. The iso-inhibition constant $K_i^{Pi\text{-}2}$, which is related to $K_d^{Pi\text{-}2}$, refers to the binding of P_i to the substrate-free enzyme, where it acts as a competitive inhibitor with respect to PEP and A5P. In the wild-type enzyme, the over 200-fold difference between $K_d^{Pi\text{-}1}$ and $K_d^{Pi\text{-}2}$ (or $K_i^{Pi\text{-}1}$ and $K_i^{Pi\text{-}2}$) clearly attests to the markedly different nature of the P_i-binding site on the substrate and product sides of the reaction and suggests that during the chemical condensation step, or upon its completion, the active site undergoes a conformational change that obliterates the binding pocket for P_i. Thus, the wild-type enzyme exists in two different forms at the start and at the end of the reaction, and an isomerization is necessary at the end of each catalytic cycle to return the enzyme to its original conformation. In contrast, there appears to be only one form of the R106G enzyme, as the observed differences between $K_d^{Pi\text{-}1}$ and $K_d^{Pi\text{-}2}$ or $K_i^{Pi\text{-}1}$ and $K_i^{Pi\text{-}2}$ are within the margin of error (Table 6).

Physiological Consequences of the R106G Substitution. During a progress curve in vitro, an enzyme system evolves from a state in which substrates are abundant and products scarce to a state in which products are abundant and substrates scarce (if the reaction, like KDO8P synthesis, is irreversible). However, in vivo, the same enzyme system will work between unchanging levels of substrates and products, as the steady-state amount of all the species in the metabolic pathway remains approximately constant over time. Knowledge of the rate constants for all the steps of a reaction can be used to simulate the enzyme behavior under conditions similar to those that might occur inside the cell. We have applied the mathematical tools of Metabolic Control Analysis (*35*−*37*), as implemented in the program Gepasi (*29*), to calculate the steady-state concentrations of the different enzyme species and the rate of KDO8P synthesis by KDO8PS. The calculation was repeated at different combinations of substrates and products concentrations to simulate the steady-state behavior of the enzyme under a wide range (1−1000 μM reactants, 1−10 000 μM products) of metabolic conditions. The result of this analysis is shown as contour surfaces in Figure 7. Each nodal point of the contour surfaces of panels A−D represents a steady-state value of the flux J(KDO8P) (μM·vol·s^{-1}) through the product release step (E·KDO8P ⇔ E + KDO8P), calculated under conditions in which the concentrations of PEP, A5P, P_i, and KDO8P (but also of all the free and bound enzyme species) remain constant over time (true steady-state). In all cases, the sum of the concentrations of all the enzyme species was 0.1 μM. When different combinations of steady-state concentrations of PEP and A5P were tested (PEP + A5P scan), the concentrations of P_i and KDO8P were kept constant at 100 μM. When different combinations of steady-state concentrations of P_i and KDO8P were tested (Pi + KDO8P scan), the concentrations of PEP and A5P were kept constant at 100 μM. The plateau of the J(KDO8P) contour surface corresponds to the range of substrates and product concentrations that are optimal for the enzyme. For the wild-type enzyme, the plateau starts at concentrations of ∼100 μM PEP and ∼60 μM A5P (Figure 7A; see iso-flux contour lines at 30%, 60%, and 90% of the plateau level projected onto the $x-y$ plane) and ends at concentrations of ∼1.6 mM P_i and ∼200 μM KDO8P (Figure 7B). For the R106G enzyme, the plateau starts at concentrations of ∼140 μM PEP and ∼500 μM A5P

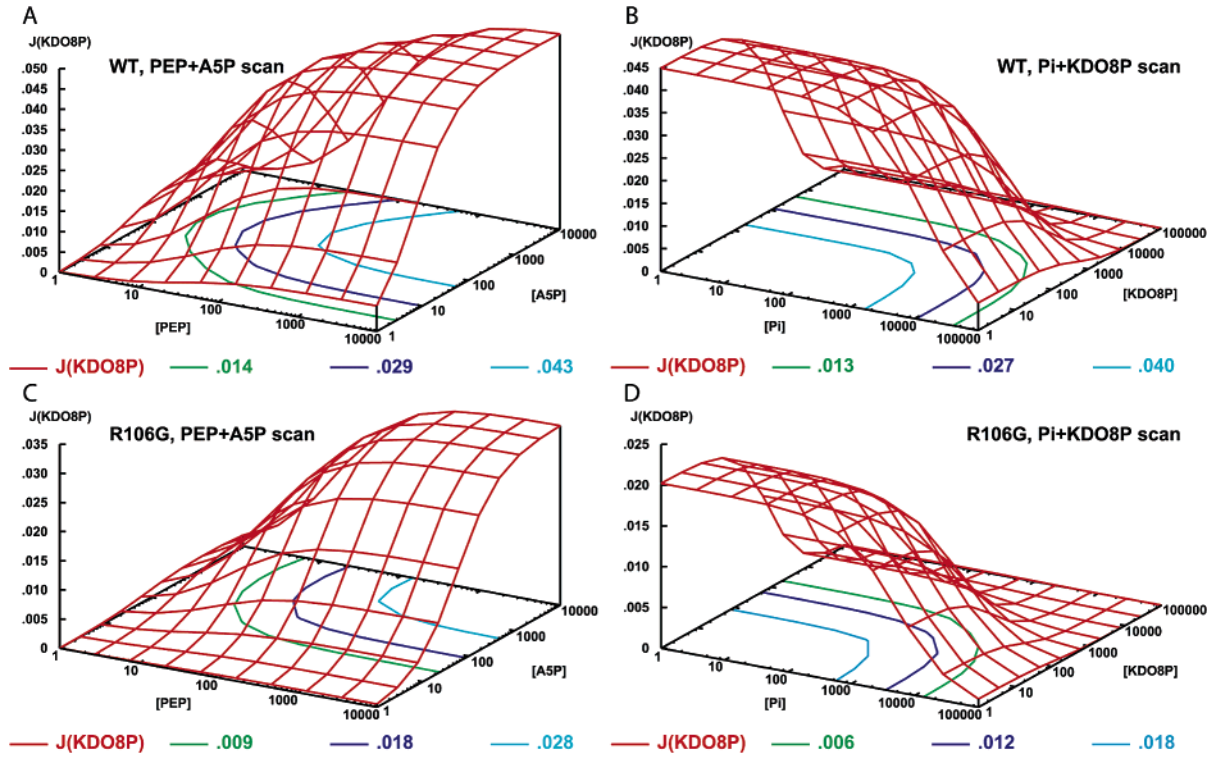

FIGURE 7: Optimal substrate/product concentrations for KDO8P synthesis. The nodal points of the contour surfaces represent steady-state values of the flux J(KDO8P) (μM·vol·s^{-1}) through the reaction step E·KDO8P ⇔ E + KDO8P. In each calculation, the enzyme concentration was 0.1 μM. Iso-flux contour lines at 30%, 60%, and 90% of the maximum value are projected onto the $x-y$ plane in the four panels. The plateaus of J(KDO8P) represent the optimal ranges of substrates and product concentrations.

and ends at concentrations of ~500 μM P_i and ~80 μM KDO8P. Thus, the mutant enzyme displays a narrower range of functionality, requiring higher concentrations of PEP and A5P and lower concentrations of P_i and KDO8P (i.e., higher sensitivity to product inhibition) to work optimally. We also notice how, at high A5P concentrations, the activity contour dips down in the wild-type but not in R106G (i.e., lower sensitivity to substrate inhibition by A5P).

^{31}P NMR of KDO8P Synthesis in the R106G Enzyme. The ~1.3-fold reduction in the k_3 rate constant observed in R106G reflects a change in the rate of the chemical step that might be a consequence of the altered equilibrium between the open and the closed form of the enzyme. The X-ray structure (see above) shows that, in R106G, the L7 loop remains disordered upon formation of the ternary complex with PEP and A5P. This observation is of special interest, as in earlier work (*2*, *3*) we have suggested that one function of the L7 loop is to prevent a "slipping" of the enzyme, which might occur if in the open form one or both substrates react with bulk water. For example, an aberrant attack by water onto $C2^{PEP}$ or $C3^{PEP}$ might lead, respectively, to the formation of pyruvate or 2-phosphoglyceric acid (2-PGA) (*38*). On this ground, one might expect some production of 2-PGA or pyruvate in the R106G mutant, in which the equilibrium between the open and closed form of the enzyme appears shifted toward the open form.

The possibility that, in the mutant enzyme, product formation might become uncoupled from substrate consumption was addressed by monitoring by ^{31}P NMR whether the conversion of substrates to products is stoichiometric. Upon incubation of the R106G enzyme (1 mM) in the presence of 5 mM PEP and 6 mM A5P for 2 h at 10 °C, only ^{31}P NMR resonances corresponding to PEP, A5P, KDO8P, and P_i could be identified (Figure 8B). At reaction completion (2.5 h), only A5P, KDO8P, and P_i were still visible (Figure 8C). At this point, pyruvate was found by enzymatic assay to be present at the concentration of 22 μM in the reaction mixture and 12 μM in a PEP standard, kept in ice for an equal length of time. These amounts can be easily accounted for by a slow nonenzymatic hydrolysis of PEP.

DISCUSSION

KDO8P synthase can exist in an open or closed state depending on the conformation of the L7 loop. In the closed state, a single conformation of the loop is stabilized by protein contacts; in the open state, the L7 loop probably exists as an ensemble of open conformations and, thus, appears disordered in the X-ray structure. The main structural abnormality of the R106G enzyme is a shift in the equilibrium between the open and closed forms of the L7 loop in favor of the open form. EDDMs between wild-type and mutant point to subtle structural changes encompassing residues 45−55 of the R106G mutant. This region corresponds to the section of the L2 loop that provides most of the interactions with the phosphate moiety of A5P. In the wild type, the L7 loop (in its closed conformation) interacts both with the phosphate moiety of A5P (through Ser^{197}) and with the L2 loop. In R106G, the L2 loop is partially open, such that A5P binds in a more peripheral position (Figure 3). Together, these two factors weaken the interactions with the L7 loop, preventing its closure. Thus, while the L7 loop is the "lid" that controls access to the active site, the L2 loop is the "latch" that locks the L7 loop in position.

Two main kinetic abnormalities were observed in R106G. On the substrate side of the reaction, PEP binds more tightly,

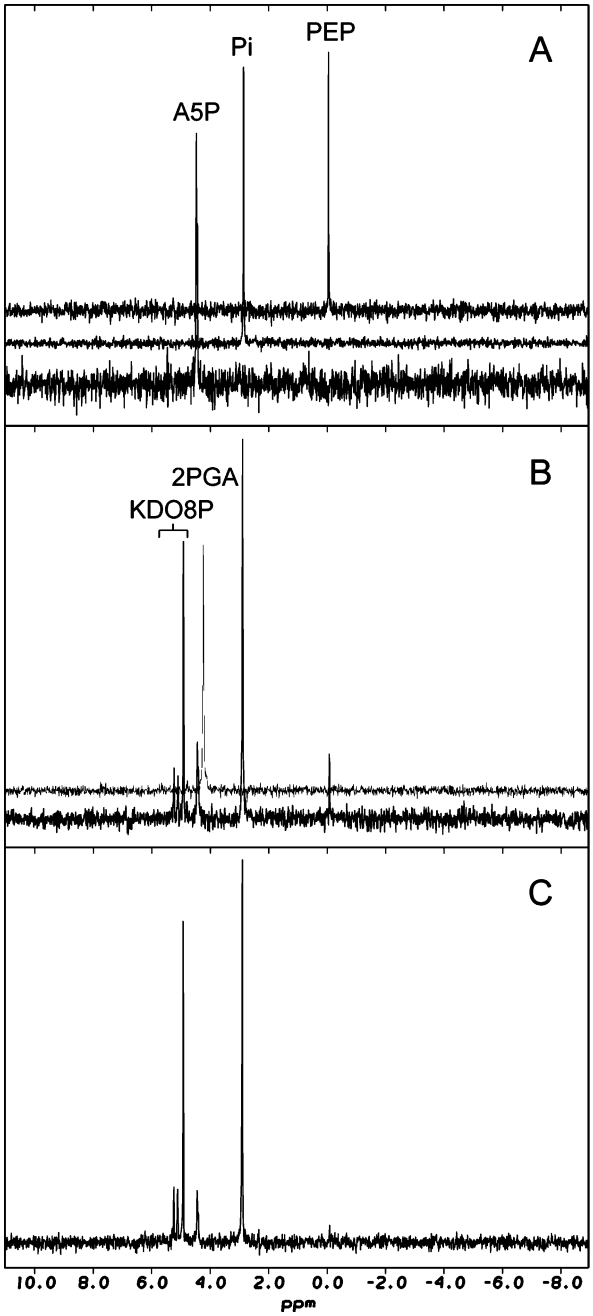

FIGURE 8: ^{31}P NMR of KDO8P synthesis in the R106G enzyme. (A) Spectra of PEP, A5P, and P_i standard. (B) Spectrum of a reaction mixture containing 50 mM Tris-Cl (pH 7.5), 10% D_2O, 1 mM R106G enzyme, 5 mM PEP, and 6 mM A5P after 2 h incubation at 10 °C. Note the presence of three resonances for KDO8P due, respectively, to the three most abundant anomers of this compound, the α-pyranose (~66%), the α-furanose (~19%), and the β-furanose (~12.0%) (*43*). The spectrum of a 2-PGA standard is superimposed. (C) Spectrum of the same reaction mixture after an additional 30 min. Note the almost complete disappearance of PEP. The observed chemical shifts (ppm) are PEP, 0.064; P_i, 2.907; A5P, 4.444; 2-PGA, 4.234; and KDO8P, 4,919, 5.105, and 5.245.

but A5P is less effective as a substrate, and therefore, it is also a weaker substrate inhibitor. On the product side of the reaction, P_i and KDO8P bind more tightly and are therefore stronger product inhibitors. It is difficult at this point to rationalize whether these changes are a direct consequence of the loss of the Arg^{106} side chain or an indirect consequence of the effects of the mutation on the dynamics of the L7 loop. At least in the case of A5P, both elements probably contribute to the decreased strength of this substrate binding. In fact, the phosphate moiety of A5P interacts with the guanidinium moiety of Arg^{106} (Figure 2) and with the backbone and side chain of Ser^{197} when the L7 loop is in the closed conformation (Figure 3).

The combined effect of all the kinetic anomalies observed in R106G is that, in the bacterial cell, this enzyme would be optimally active in a narrower range of metabolic conditions, requiring higher concentrations of PEP and A5P and lower concentrations of P_i (Figure 7). It should also be noticed that, at concentrations of PEP and A5P that appear more likely (around 100 μM), the mutant enzyme would achieve at best 44% of the wild-type activity at any concentration of P_i and KDO8P (see Figure 7B,D), despite the fact that its k_{cat} is 67% of the wild-type value. This observation perhaps explains why an arginine residue is universally conserved at this position in all KDO8PSs. It can also be argued that the range of substrate and product concentrations that is best for the wild-type enzyme provides an indication of the concentrations of these metabolites in vivo. However, our studies were carried out at 40 °C, while *A. aeolicus* grows optimally at 85 °C. As the temperature dependence of the activation energy might be different for different reaction steps, additional kinetic studies at both lower and higher temperatures are necessary before a conclusion can be reached on this point.

Many enzymes display a conformational equilibrium between open and closed forms. In some, loop closure brings new catalytic groups for the recognition of substrates or the stabilization of transition states (e.g., lactate dehydrogenase (*39*), Rubisco (*40*), aldolase (*41*)). In triose phosphate isomerase (TIM), the archetype of TIM barrel proteins, closure of the L6 loop does not provide catalytic residues but prevents the escape from the active site of an enediol phosphate intermediate that otherwise would decompose in solution eliminating phosphate (*42*). As KDO8P synthesis proceeds through the formation of a transient intermediate (Figure 1), one may ask whether the L7 loop of KDO8PS, which also provides no catalytic residues, might have a function similar to the L6 loop of TIM. However, no species other than PEP, A5P, P_i, and KDO8P were detected by means of ^{31}P NMR during the course of KDO8P synthesis by R106G. While this observation does not rule out that small amounts of the intermediate (below the detection threshold of the NMR spectrometer) might escape the active site, it suggests that this phenomenon does not account for a massive slippage of the enzyme. Consistent with this observation, the intrinsic rate of the chemical step (k_3) determined by progress curve analysis decreases only by a factor of 1.5 in R106G, although the L7 loop remains open for a longer time than in the wild-type enzyme during the catalytic cycle.

Kinetic analysis of the progress curves suggests that in the wild-type there are two forms of the enzyme (which we might refer to here as E and E*) characterized by different affinities for P_i (Table 6). P_i acts as a competitive inhibitor of E ($K_i^{Pi\text{-}2}$, Table 6), and as an uncompetitive inhibitor of E* ($K_i^{Pi\text{-}1}$, Table 6). At the start of the reaction, E binds P_i tightly ($K_d^{Pi\text{-}2}$, $K_i^{Pi\text{-}2}$, Table 6), while upon completion of the condensation step, the P_i-binding site is obliterated ($K_d^{Pi\text{-}1}$, $K_i^{Pi\text{-}1}$, Table 6). Conversion of E to E* probably occurs during or immediately after the condensation step. An isomerization

step is necessary to return E* to E. In contrast, in R106G, there appears to be only one form of the enzyme with respect to P_i binding (Table 6). This observation is of particular interest, in view of the fact that there is crystallographic evidence that the enzyme might work by alternating catalysis between two different subunits (*2*, *3*). Catalysis would occur at the active site in which both substrates bind (Figure 2), while the other site, where only PEP binds, would wait for its turn in the next cycle. Arg106 is the only residue of each subunit that extends inside the active site of the other subunit and, thus, is the ideal candidate to play a regulatory role in the alternation of catalysis between subunits. With respect to this point, it is worth noting that alternation of catalysis might be a convenient avenue to couple the free-energy change associated with A5P binding, at the site that will turn over next, to the isomerization of E* to E at the site that just finished its cycle. This hypothesis is particularly suggestive in view of the fact that Arg^{106} is also directly involved in the binding of A5P (Figures 2 and 3). The methodology of kinetic analysis applied here for the first time to the study of KDO8PS provides an additional powerful tool for the future testing of this hypothesis through kinetic models that include explicitly both the alternation of catalysis between subunits and the isomerization between different forms of the enzyme.

ACKNOWLEDGMENT

We thank Dr. Sharon Ackerman for her critical evaluation of the manuscript.

REFERENCES

1. Levin, D. H., and Racker, E. (1959) Condensation of arabinose 5-phosphate and phosphorylenol pyruvate by 2-keto-3-deoxy-phosphooctonic acid synthetase, *J. Biol. Chem. 234*, 2532−2539.
2. Duewel, H. S., Radaev, S., Wang, J., Woodard, R. W., and Gatti, D. L. (2001) Substrate and metal complexes of 3-deoxy-D-manno-octulosonate 8-phosphate synthase from *Aquifex aeolicus* at 1.9 Å resolution: implications for the condensation mechanism, *J. Biol. Chem. 276*, 8393−8402.
3. Wang, J., Duewel, H. S., Woodard, R. W., and Gatti, D. L. (2001) Structures of *Aquifex aeolicus* KDO8P synthase in complex with R5P and PEP, and with a bisubstrate inhibitor: role of active site water in catalysis, *Biochemistry 40*, 15676−15683.
4. Asojo, O., Friedman, J., Adir, N., Belakhov, V., Shoham, Y., and Baasov, T. (2001) Crystal structures of KDOP synthase in its binary complexes with the substrate phosphoenolpyruvate and with a mechanism-based inhibitor, *Biochemistry 40*, 6326−6334.
5. Hedstrom, L., and Abeles, R. (1988) 3-Deoxy-D-manno-octulosonate-8-phosphate synthase catalyzes the C−O bond cleavage of phosphoenolpyruvate, *Biochem. Biophys. Res. Commun. 157*, 816−820.
6. Raetz, C. R. (1990) Biochemistry of endotoxins, *Annu. Rev. Biochem. 59*, 129−170.
7. Raetz, C. R., and Whitfield, C. (2002) Lipopolysaccharide endotoxins, *Annu. Rev. Biochem. 71*, 635−700.
8. Birck, M. R., and Woodard, R. W. (2001) *Aquifex aeolicus* 3-deoxy-D-manno-2-octulosonic acid 8-phosphate synthase: a new class of KDO 8-P synthase?, *J. Mol. Evol. 52*, 205−214.
9. Duewel, H. S., and Woodard, R. W. (2000) A metal bridge between two enzyme families. 3-Deoxy-D-manno-octulosonate 8-phosphate synthase from *Aquifex aeolicus* requires a divalent metal for activity, *J. Biol. Chem. 275*, 22824−22831.
10. Wu, J., Patel, M. A., Sundaram, A. K., and Woodard, R. W. (2004) Functional and biochemical characterization of a recombinant *Arabidopsis thaliana* 3-deoxy-D-manno-octulosonate 8-phosphate synthase, *Biochem. J. 381*, 185−193.
11. Duewel, H. S., Sheflyan, G. Y., and Woodard, R. W. (1999) Functional and biochemical characterization of a recombinant 3-deoxy-D-manno-octulosonic acid 8-phosphate synthase from the hyperthermophilic bacterium *Aquifex aeolicus*, *Biochem. Biophys. Res. Commun. 263*, 346−351.
12. Otwinowski, Z., and Minor, W. (1997) Processing of X-ray diffraction data collected in oscillation mode, *Methods Enzymol. 276*, 307−326.
13. Adams, P. D., Pannu, N. S., Read, R. J., and Brunger, A. T. (1997) Cross-validated maximum likelihood enhances crystallographic simulated annealing refinement, *Proc. Natl. Acad. Sci. U.S.A. 94*, 5018−5023.
14. Schneider, T. R. (2000) Objective comparison of protein structures: error-scaled difference distance matrices, *Acta Crystallogr., Sect. D 56* (Pt 6), 714−721.
15. Schneider, T. R. (2002) A genetic algorithm for the identification of conformationally invariant regions in protein molecules, *Acta Crystallogr., Sect. D 58*, 195−208.
16. Cruickshank, D. W. (1999) Remarks about protein structure precision, *Acta Crystallogr., Sect. D 55* (Pt 3), 583−601.
17. Hadjivassiliou, A. G., and Rieder, S. V. (1968) The enzymatic assay of pyruvic and lactic acids. A definitive procedure, *Clin. Chim. Acta 19*, 357−361.
18. Duggleby, R. G. (1995) Analysis of enzyme progress curves by nonlinear regression, *Methods Enzymol. 249*, 61−90.
19. Kohen, A., Jakob, A., and Baasov, T. (1992) Mechanistic studies of 3-deoxy-D-manno-2-octulosonate-8-phosphate synthase from *Escherichia coli*, *Eur. J. Biochem. 208*, 443−449.
20. Baasov, T., Sheffer-Dee-Noor, S., Kohen, A., Jakob, A., and Belakhov, V. (1993) Catalytic mechanism of 3-deoxy-D-manno-2-octulosonate-8-phosphate synthase. The use of synthetic analogues to probe the structure of the putative reaction intermediate, *Eur. J. Biochem. 217*, 991−999.
21. Liang, P. H., Lewis, J., Anderson, K. S., Kohen, A., D'Souza, F. W., Benenson, Y., and Baasov, T. (1998) Catalytic mechanism of Kdo8P synthase: transient kinetic studies and evaluation of a putative reaction intermediate, *Biochemistry 37*, 16390−16399.
22. Dotson, G. D., Dua, R. K., Clemens, J. C., Wooten, E. W., and Woodard, R. W. (1995) Overproduction and one-step purification of *Escherichia coli* 3-deoxy-D-manno-octulosonic acid 8-phosphate synthase and oxygen transfer studies during catalysis using isotopic-shifted heteronuclear NMR, *J. Biol. Chem. 270*, 13698−13705.
23. Dotson, G. D., Nanjappan, P., Reily, M. D., and Woodard, R. W. (1993) Stereochemistry of 3-deoxyoctulosonate 8-phosphate synthase, *Biochemistry 32*, 12392−12397.
24. Kuzmic, P. (1996) Program DYNAFIT for the analysis of enzyme kinetic data: application to HIV proteinase, *Anal.Biochem. 237*, 260−273.
25. King, E. L., and Altman, C. (1956) A Schematic method of deriving the rate laws for enzyme-catalyzed reactions, *J. Phys. Chem. 60*, 1375−1378.
26. Segel, I. (1975) *Enzyme Kinetics. Behavior and Analysis of Rapid Equilibrium and Steady-State Enzyme Systems*, John Wiley & Sons, Inc., New York.
27. Cornish-Bowden, A. (1977) An automatic method for deriving steady-state rate equations, *Biochem. J. 165*, 55−59.
28. Cleland, W. W. (1963) The kinetics of enzyme-catalyzed reactions with two or more substrates or products. I. Nomenclature and rate equations, *Biochim. Biophys. Acta 67*, 104−137.
29. Mendes, P. (1993) GEPASI: a software package for modelling the dynamics, steady states and control of biochemical and other systems, *Comput. Appl. Biosci. 9*, 563−571.
30. Hindmarsh, A. C. (1983) ODEPACK: a systematized collection of ODE solvers, in *Scientific Computing* (Stepleman, R. S., Ed.) pp 55−64, North-Holland, Amsterdam.
31. Kohen, A., Berkovich, R., Belakhov, V., and Baasov, T. (1993) Stereochemistry of KDO8P synthase. An efficient synthesis of the 3-fluoro analogs of KDO8P, *Bioorg. Med. Chem. Lett. 3*, 1577−1582.
32. Snee, R. D. (1977) Validation of regression models: methods and examples, *Technometrics 19* (4), 415−428.
33. Efron, B. (1983) Estimating the error rate of a prediction rule: improvement on cross-validation, *J. Am. Stat. Assoc. 78*, 316−331.
34. Fersht, A. (1999) *Structure and Mechanism in Protein Science: A Guide to Enzyme Catalysis and Protein Folding*, W H Freeman & Co, New York.

35. Kacser, H., and Burns, J. A. (1995) The control of flux, *Biochem. Soc. Trans. 23*, 341−366.
36. Brown, G. C., Westerhoff, H. V., and Kholodenko, B. N. (1996) Molecular control analysis: control within proteins and molecular processes, *J. Theor. Biol. 182*, 389−396.
37. Kholodenko, B. N., and Westerhoff, H. V. (1994) Control theory of one enzyme, *Biochim. Biophys. Acta 1208*, 294−305.
38. Howe, D. L., Sundaram, A. K., Wu, J., Gatti, D. L., and Woodard, R. W. (2003) Mechanistic insight into 3-deoxy-D-manno-octulosonate-8-phosphate synthase and 3-deoxy-D-arabino-heptulosonate-7-phosphate synthase utilizing phosphorylated monosaccharide analogues, *Biochemistry 42*, 4843−4854.
39. Clarke, A. R., Wigley, D. B., Chia, W. N., Barstow, D., Atkinson, T., and Holbrook, J. J. (1986) Site-directed mutagenesis reveals role of mobile arginine residue in lactate dehydrogenase catalysis, *Nature 324*, 699−702.
40. Andersson, I., and Taylor, T. C. (2003) Structural framework for catalysis and regulation in ribulose-1,5-bisphosphate carboxylase/oxygenase, *Arch. Biochem. Biophys. 414*, 130−140.
41. Zgiby, S., Plater, A. R., Bates, M. A., Thomson, G. J., and Berry, A. (2002) A functional role for a flexible loop containing Glu182 in the class II fructose-1,6-bisphosphate aldolase from *Escherichia coli*, *J. Mol. Biol. 315*, 131−140.
42. Pompliano, D. L., Peyman, A., and Knowles, J. R. (1990) Stabilization of a reaction intermediate as a catalytic device: definition of the functional role of the flexible loop in triosephosphate isomerase, *Biochemistry 29*, 3186−3194.
43. Kaustov, L., Baasov, T., and Schmidt, A. (2003) Binding of the natural substrates and products to KDO8P synthase: 31P and 13C solution NMR characterization, *Bioorg. Chem. 31*, 306−321.

BI051095Q